



Aerosol pH and its driving factors in Beijing

Jing Ding², Pusheng Zhao¹, Jie Su¹, Qun Dong^{1,3}, Xiang Du^{2,1}, and Yufen Zhang²

¹Institute of Urban Meteorology, China Meteorological Administration, Beijing 100089, China

²State Environmental Protection Key Laboratory of Urban Ambient Air Particulate Matter Pollution Prevention and Control, College of Environmental Science and Engineering, Nankai University, Tianjin 300071, China

³Beilun Bureau of Meteorology, Ningbo 315800, China

Correspondence: Pusheng Zhao (pszhao@ium.cn)

Received: 13 March 2018 – Discussion started: 14 May 2018

Revised: 24 May 2019 – Accepted: 3 June 2019 – Published: 17 June 2019

Abstract. Aerosol acidity plays a key role in secondary aerosol formation. The high-temporal-resolution PM_{2.5} pH and size-resolved aerosol pH in Beijing were calculated with ISORROPIA II. In 2016–2017, the mean PM_{2.5} pH (at relative humidity (RH) > 30 %) over four seasons was 4.5 ± 0.7 (winter) > 4.4 ± 1.2 (spring) > 4.3 ± 0.8 (autumn) > 3.8 ± 1.2 (summer), showing moderate acidity. In coarse-mode aerosols, Ca²⁺ played an important role in aerosol pH. Under heavily polluted conditions, more secondary ions accumulated in the coarse mode, leading to the acidity of the coarse-mode aerosols shifting from neutral to weakly acidic. Sensitivity tests also demonstrated the significant contribution of crustal ions to PM_{2.5} pH. In the North China Plain (NCP), the common driving factors affecting PM_{2.5} pH variation in all four seasons were SO₄^{2−}, TNH₃ (total ammonium (gas + aerosol)), and temperature, while unique factors were Ca²⁺ in spring and RH in summer. The decreasing SO₄^{2−} and increasing NO₃[−] mass fractions in PM_{2.5} as well as excessive NH₃ in the atmosphere in the NCP in recent years are the reasons why aerosol acidity in China is lower than that in Europe and the United States. The nonlinear relationship between PM_{2.5} pH and TNH₃ indicated that although NH₃ in the NCP was abundant, the PM_{2.5} pH was still acidic because of the thermodynamic equilibrium between NH₄⁺ and NH₃. To reduce nitrate by controlling ammonia, the amount of ammonia must be greatly reduced below excessive quantities.

1 Introduction

Aerosol acidity has a significant effect on secondary aerosol formation through the gas–aerosol partitioning of semi-volatile and volatile species (Eddingsaas et al., 2010; Surratt et al., 2010; Pathak et al., 2011; Guo et al., 2016). Studies have shown that aerosol acidity can promote the generation of secondary organic aerosols by affecting aerosol acid-catalyzed reactions (Rengarajan et al., 2011). Moreover, metals can become soluble by acid dissociation under low aerosol pH (Shi et al., 2011; Meskhidze et al., 2003; Fang et al., 2017) or by forming ligands with organic species, such as oxalate, at higher pH (Schwertmann et al., 1991). The investigation of aerosol acidity is conducive to better understanding the important role of aerosols in acid deposition and atmospheric chemical reactions.

Aerosol acidity is frequently estimated by the charge balance of measurable cations and anions. Nevertheless, not all ions (even trace ones) are well constrained in the observations and the dissociation state of multivalent ions is unclear. Ion balance and other similar proxies fail to represent the in situ aerosol pH because such metrics cannot accurately predict the H⁺ concentration in the aerosol liquid phase (Guo et al., 2015; Hennigan et al., 2015). To better understand the in situ aerosol pH, the aerosol liquid water content (ALWC) and hydrogen ion concentration per volume air (H_{air}⁺) should be determined (Guo et al., 2015).

Most inorganic ions and some organic acids in aerosols are water soluble (Peng, 2001; Wang et al., 2017). Since the deliquescence relative humidity (DRH) and the efflorescence relative humidity (ERH) of mixed salts are lower than that of any single component, ambient aerosols are gener-

ally in the form of droplets containing liquid water (Seinfeld and Pandis, 2016). ALWC can be derived from hygroscopic growth factors or calculated by thermodynamic models, and good consistencies in ALWC have been found among these methods (Engelhart et al., 2011; Bian et al., 2014; Guo et al., 2015). However, H_{air}^+ can only be obtained by thermodynamic models, which offer a more precise approach to determine aerosol pH (Nowak et al., 2006; Fountoukis et al., 2009; Weber et al., 2016; Fang et al., 2017). Among these thermodynamic models, ISORROPIA II is widely used owing to its rigorous calculation, performance, and computational speed (Guo et al., 2015; Fang et al., 2017; Liu et al., 2017; Galon-Negru et al., 2018).

The North China Plain (NCP) is the region with the most severe aerosol pollution in China. Nitrate and sulfate are the major contributors to haze, and their secondary formation processes are determined in large part by aerosol pH (Zou et al., 2018; Huang et al., 2017; Gao et al., 2018). Therefore, understanding the aerosol pH level in this region is extremely important and has recently become a trending topic. Fine aerosol pH reported in the NCP (Liu et al., 2017; Song et al., 2018; Shi et al., 2017, 2019) was higher than that found in the United States or Europe, where aerosols are often highly acidic with a pH lower than 3.0 (Guo et al., 2015, 2016; Bougiatioti et al., 2016; Weber et al., 2016; Young et al., 2013). The differences in aerosol pH in the NCP arise from (1) different methods or different model settings, (2) variations in $\text{PM}_{2.5}$ chemical composition in the NCP in recent years, (3) the levels of gas precursors of the main water-soluble ions (NH_3 , HNO_3 , and HCl), and (4) differences in ambient temperature and RH. Studies demonstrated that pH diurnal variations are largely driven by meteorological conditions (Guo et al., 2015, 2016; Bougiatioti et al., 2016). In the NCP, a comprehensive understanding of the impacts of these factors on aerosol pH is still poor.

Additionally, most studies on aerosol pH focus on PM_{10} or $\text{PM}_{2.5}$. Knowledge regarding size-resolved aerosol pH is still rare (Fang et al., 2017; Craig et al., 2018). Aerosol chemical compositions are different among multiple size ranges. Among inorganic ions, SO_4^{2-} , NO_3^- , Cl^- , K^+ , and NH_4^+ are mainly concentrated in the fine mode except on dusty days (Meier et al., 2009; Pan et al., 2009; Tian et al., 2014), whereas Mg^{2+} and Ca^{2+} are abundant in the coarse mode (Zhao et al., 2017). Aerosol pH can be expected to be diverse among different particle sizes; pH levels at different sizes may be associated with different formation pathways of secondary aerosols.

To better understand the driving factors of aerosol acidity, in this work, the thermodynamic model ISORROPIA II was utilized to predict aerosol pH in Beijing based on a long-term online high-temporal-resolution dataset and a size-resolved offline dataset. The hourly measured $\text{PM}_{2.5}$ inorganic ions and precursor gases in four seasons from 2016 to 2017 were used to analyze the seasonal and diurnal variations in aerosol acidity; samples collected by multistage cas-

cade impactors (MOUDI-120) were used to estimate the pH variations among 10 different size ranges. Additionally, a sensitivity analysis was conducted to identify the key factors affecting aerosol pH and gas–particle partitioning. The main purposes of this work are to (1) obtain the $\text{PM}_{2.5}$ pH level based on an online measurement, contributing towards a global pH dataset; (2) investigate the size-resolved aerosol pH, providing useful information for understanding the formation processes of secondary aerosols; and (3) explore the main factors affecting aerosol pH and gas–particle partitioning, which can help explain the possible reasons for pH divergence in different works and provide a basis for controlling secondary aerosol generation.

2 Data collection and methods

2.1 Site

The measurements were performed at the Institute of Urban Meteorology in the Haidian district of Beijing ($39^\circ 56' \text{ N}$, $116^\circ 17' \text{ E}$). The site is located next to a high-density residential area, without significant nearby air pollution emissions. Therefore, the observation data represent the air quality levels of the urban area of Beijing.

2.2 Online data collection

Water-soluble ions (SO_4^{2-} , NO_3^- , Cl^- , NH_4^+ , Na^+ , K^+ , Mg^{2+} , and Ca^{2+}) in $\text{PM}_{2.5}$ and gaseous precursors (HCl , HNO_3 , HNO_2 , SO_2 , and NH_3) in ambient air were measured by an online analyzer (MARGA) with hourly temporal resolution during spring (April and May 2016), winter (February 2017), summer (July and August 2017), and autumn (September and October 2017). More details about MARGA can be found in Rumsey et al. (2014) and Chen et al. (2017). The $\text{PM}_{2.5}$ and PM_{10} mass concentrations (TEOM 1405-DF), hourly ambient temperature, and RH were also synchronously obtained. The hourly concentrations of $\text{PM}_{2.5}$, PM_{10} , and major secondary ions (SO_4^{2-} , NO_3^- , and NH_4^+) in $\text{PM}_{2.5}$, as well as meteorological parameters during the observations, are shown in Fig. 1. In the spring, two dust events occurred (21 April and 6 May). In the following pH analysis based on MARGA data, it was assumed that the particles were internally mixed; hence, these two dust events were excluded from this analysis.

2.3 Size-resolved chemical composition

A micro-orifice uniform deposit impactor (MOUDI-120) was used to collect size-resolved aerosol samples with calibrated 50 % cut sizes of 0.056, 0.10, 0.18, 0.32, 0.56, 1.0, 1.8, 3.1, 6.2, 9.9, and $18 \mu\text{m}$. Size-resolved sampling was conducted 12–18 July 2013, 13–19 January 2014, 3–5 July 2014, 9–20 October 2014, and 26–28 January 2015. A total of 15, 14, and 18 sets of samples were obtained in summer, au-

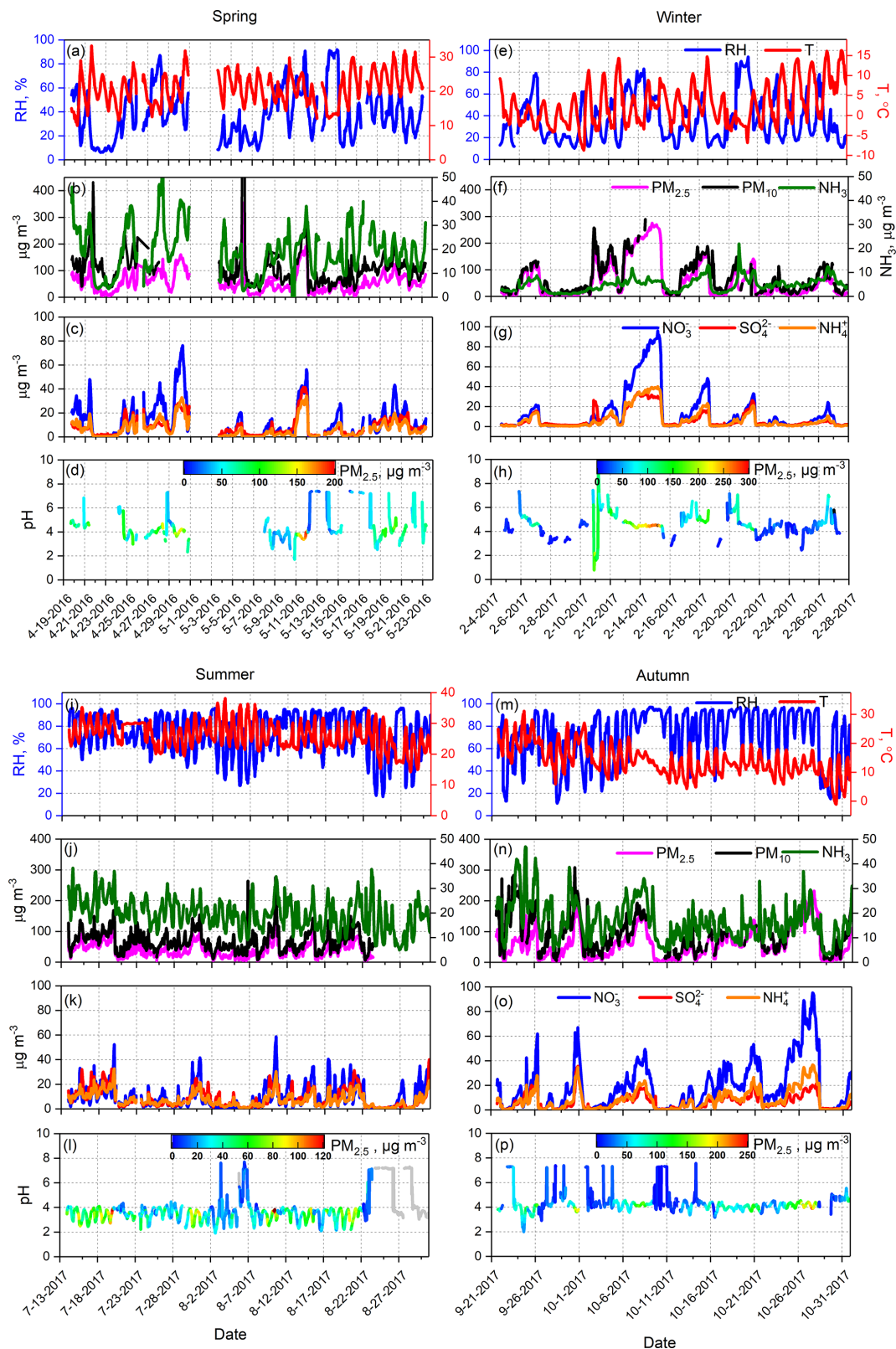


Figure 1. Time series of relative humidity (RH) and temperature (T) (a, e, i, m); $\text{PM}_{2.5}$, PM_{10} , and NH_3 (b, f, j, n); dominant water-soluble ions: NO_3^- , SO_4^{2-} , and NH_4^+ (c, g, k, o); and $\text{PM}_{2.5}$ pH colored by $\text{PM}_{2.5}$ concentration (d, h, l, p) over four seasons.

tumn, and winter, respectively. Except for two sets of samples, all the samples were collected in daytime (from 08:00 to 19:00 LST) and nighttime (from 20:00 to 07:00 LST the next day). A total of 1 h of preparation time was allowed for filter changing and washing the nozzle plate with ethanol. The water-soluble ions in the samples were analyzed by using ion chromatography (DIONEX ICS-1000). Detailed information about the features of MOUDI-120 and the procedures of sampling, pre-treatment, and laboratory chemical analysis (including quality assurance and quality control) were described in our previous papers (Zhao et al., 2017; Su et al., 2018).

2.4 Aerosol pH prediction

Aerosol pH can be predicted by thermodynamic models such as AIM and ISORROPIA (Clegg et al., 1998; Nenes et al., 1998). AIM is considered an accurate benchmark model, while ISORROPIA has been optimized for use in chemical transport models. Currently, ISORROPIA II, with the addition of K^+ , Mg^{2+} , and Ca^{2+} (Fountoukis and Nenes, 2007), can calculate the equilibrium H_{air}^+ and ALWC with reasonable accuracy by using the water-soluble ion mass concentration, temperature (T), and RH as input. H_{air}^+ and ALWC were then used to predict aerosol pH by Eq. (1).

$$pH = -\log_{10} H_{aq}^+ \cong -\log_{10} \frac{1000 H_{air}^+}{ALWC_i}, \quad (1)$$

where H_{aq}^+ (mol L^{-1}) is the hydronium ion concentration in the ambient particle liquid water. H_{aq}^+ can also be calculated as H_{air}^+ ($\mu\text{g m}^{-3}$) divided by the concentration of ALWC associated with inorganic species, $ALWC_i$ ($\mu\text{g m}^{-3}$). Both the inorganic species and part of the organic species in particles are hygroscopic. However, pH prediction is not highly sensitive to water uptake by organic species ($ALWC_o$) (Guo et al., 2015, 2016). In recent years, the fraction of organic matter in $PM_{2.5}$ in the NCP was 20 %–25 %, which is much lower than that in the United States (Guo et al., 2015). In contrast, approximately 50 % of $PM_{2.5}$ in the NCP is inorganic ions (Huang et al., 2017; Zhang et al., 2018, 2019). The results obtained by Liu et al. (2017) in Beijing showed that the mass fraction of organic-matter-induced particle water accounted for only 5 % of total ALWC, indicating a negligible contribution to aerosol pH. Hence, aerosol pH can be fairly well predicted by ISORROPIA II with only measurements of inorganic species in most cases. However, potential errors can be incurred by ignoring $ALWC_o$ in regions where hygroscopic organic species have a relatively high contribution to fine particles.

In ISORROPIA II, forward and reverse modes are provided to predict ALWC and H_{air}^+ . In forward mode, T , RH, and the total (i.e., gas + aerosol) concentrations of NH_3 , H_2SO_4 , HCl , and HNO_3 need to be input. In reverse mode, equilibrium partitioning is calculated given only the concentrations of aerosol components, RH, and T as input. In this

work, the online ion chromatography system MARGA was used to measure both inorganic ions in $PM_{2.5}$ and gaseous precursors. Moreover, the forward mode has been reported to be less sensitive to measurement error than the reverse mode (Hennigan et al., 2015; Song et al., 2018). Hence, ISORROPIA II was run in forward mode for aerosols in the metastable conditions in this study.

When using ISORROPIA II to calculate the $PM_{2.5}$ acidity, all particles were assumed to be internally mixed, and the bulk properties were used without considering the variability in chemical composition at a given particle size. In the ambient atmosphere, the aerosol chemical composition is complicated; hence, the deliquescence relative humidity (DRH) of aerosols is generally low (Seinfeld and Pandis, 2016). Once the particles are deliquescent, crystallization only occurs at a very low RH, which is called the hysteresis phenomenon. The efflorescence RH (ERH) of a salt cannot be calculated from thermodynamic principles; rather, it must be measured in the laboratory. For a particle consisting of approximately 1 : 1 (NH_4)₂SO₄ : NH_4NO_3 , the ERH is around 20 %, while for a 1 : 2 molar ratio it decreases to around 10 % (Shaw and Rood, 1990). Recently, NO_3^- has dominated the particles in the NCP (Zhao et al., 2013, 2017; Huang et al., 2017; Ma et al., 2017); therefore, we assumed that the particles are in a liquid state (metastable condition). Assumptions that particles are metastable were adopted by numerous studies in the NCP (Liu et al., 2017; Guo et al., 2017; Shi et al., 2017, 2019). Figures 2 and S1–S4 in the Supplement show comparisons between the predicted and measured NH_3 , HNO_3 , HCl , NH_4^+ , NO_3^- , Cl^- , $\varepsilon(NH_4^+)$ ($NH_4^+ / (NH_3 + NH_4^+)$, mol / mol), $\varepsilon(NO_3^-)$ ($NO_3^- / (HNO_3 + NO_3^-)$, mol / mol), and $\varepsilon(Cl^-)$ ($Cl^- / (HCl + Cl^-)$, mol / mol) based on real-time ion chromatography data; all results are colored with the corresponding RH. The predicted and measured NH_3 , NH_4^+ , NO_3^- , and Cl^- values are in good agreement: the R^2 values of linear regressions are all higher than 0.94, and the slopes are approximately 1. Moreover, the agreement between the predicted and measured $\varepsilon(NH_4^+)$ is better than that of $\varepsilon(NO_3^-)$ and $\varepsilon(Cl^-)$. The slope of the linear regression between the predicted and measured $\varepsilon(NH_4^+)$ was 0.93, 0.91, 0.95, and 0.96 and R^2 was 0.87, 0.93, 0.89, and 0.97 in spring, winter, summer, and autumn, respectively. However, the measured and predicted partitioning of HNO_3 and HCl show significant discrepancies (R^2 values of 0.28 and 0.18, respectively), which may be attributed to the much lower gas concentrations than particle concentrations, as well as the HNO_3 and HCl measurement uncertainties from MARGA (Rumsey et al., 2014). Clearly, more scatter points deviate from the 1 : 1 line when ISORROPIA II is operated at $RH \leq 30$ %, which is highly evident in winter and spring. It should be noted that when RH is low, ALWC becomes very small, and $PM_{2.5}$ pH is subject to considerably more uncertainty. Guo et al. (2016) suggest that the lower RH limit is about 40 %. In this work, due to the overall good agreement between predictions and

measurements when RH was higher than 30 %, we only determined the PM_{2.5} pH for data with RH higher than 30 %.

Running ISORROPIA II in the forward mode with only aerosol component concentrations as input may result in a bias in predicted pH due to repartitioning of ammonia in the model, leading to a lower predicted pH when gas-phase data are not available (Hennigan et al., 2015). In this work, no synchronous gas phase was available during the MOUDI sampling periods; the gas-phase measurements that were taken by the MARGA in 2017 were therefore applied. Even if the periods were not perfectly aligned, the order of magnitude of NH₃, HNO₃, and HCl during a certain period did not change drastically. Guo et al. (2017) found that even if there was some error in NH₃, pH was less sensitive to it; a change with a factor of 10 in NH₃ was required to change pH by 1 unit. Averaged values of NH₃, HNO₃, and HCl measured by MARGA matched to PM_{2.5} mass concentration levels during the MOUDI sampling periods. Together with ion concentrations of samples collected by MOUDI, the average RH and *T* during each sampling period were used to determine the aerosol pH for different size ranges. Similar to calculating the PM_{2.5} pH, it was assumed that all the particles in each size bin were internally mixed and had the same pH.

Comparisons of the measured and predicted NO₃⁻, NH₄⁺, and Cl⁻ for MOUDI samples are shown in Fig. 3. The measured and predicted NO₃⁻, NH₄⁺, and Cl⁻ agreed very well in fine-mode particles; the slopes are approximately 1. In the coarse mode, the predicted NH₄⁺ was lower than the measured NH₄⁺ due to the impact of crustal ions.

2.5 Sensitivity of PM_{2.5} pH to SO₄²⁻, TNO₃, TNH₃, Ca²⁺, RH, and *T*

To explore the major influencing factors on aerosol pH, sensitivity tests were performed. In the sensitivity analysis, SO₄²⁻, TNO₃ (total nitrate (gas + aerosol) expressed as equivalent HNO₃), TNH₃ (total ammonium (gas + aerosol) expressed as equivalent NH₃), Ca²⁺, RH, and *T* were selected as the variables since SO₄²⁻ and NO₃⁻ are major anions in aerosols, NH₄⁺ and Ca²⁺ are major cations in aerosols, and Ca²⁺ is generally considered representative of crustal ions. To assess how a variable affects PM_{2.5} pH, the real-time measured values of this variable and the average values of other species (K, Na, Mg, and total chloride (gas + aerosol) were also included) in each season were input into ISORROPIA II. The magnitude of the relative standard deviation (RSD) of the calculated aerosol pH can reflect the impact of variable variations on aerosol acidity. The higher the RSD is, the greater the impact, and vice versa. The average value and variation range for each variable in the four seasons are listed in Table S1 in the Supplement.

The sensitivity analysis in this work was only aimed at PM_{2.5} (i.e., fine particles) since the MARGA system equipped with a PM_{2.5} inlet had a high temporal resolution (1 h). In addition, the dataset had a wide range, covering dif-

ferent levels of haze events. The sensitivity analysis in this work only reflected the characteristics during the observation periods, and further work is needed to determine whether the sensitivity analysis is valid in other environments.

3 Results and discussion

3.1 Overall summary of PM_{2.5} pH over four seasons

The average mass concentrations of PM_{2.5} and major inorganic ions in the four seasons are shown in Table 1. Among all the ions measured, NO₃⁻, SO₄²⁻, and NH₄⁺ were the three most dominant species, accounting for 83 %–87 % of the total ion content. The average concentrations of primary inorganic ions (Cl⁻, Na⁺, K⁺, Mg²⁺, and Ca²⁺) were higher in spring than in other seasons. PM_{2.5} in Beijing showed moderate acidity, with PM_{2.5} pH values of 4.4 ± 1.2, 4.5 ± 0.7, 3.8 ± 1.2, and 4.3 ± 0.8 for spring, winter, summer, and autumn observations, respectively (data at RH ≤ 30 % were excluded). The overall winter PM_{2.5} pH was comparable to the result (4.2) found in Beijing by Liu et al. (2017) and that (4.5) found by Guo et al. (2017), but lower than that (4.9, winter and spring) in Tianjin (Shi et al., 2017), another megacity approximately 120 km away from Beijing. The PM_{2.5} pH in summer was lowest among all four seasons. The seasonal variation in PM_{2.5} pH in this work was similar to the results in Tan et al. (2018), except for spring, and followed the trend of winter (4.11 ± 1.37) > autumn (3.13 ± 1.20) > spring (2.12 ± 0.72) > summer (1.82 ± 0.53).

To further investigate the PM_{2.5} pH level under different pollution conditions over four seasons, the PM_{2.5} concentrations were classified into three groups: 0–75, 75–150, and > 150 µg m⁻³, representing clean, polluted, and heavily polluted conditions, respectively. The relationship between PM_{2.5} concentration and pH is shown in Fig. S5. The PM_{2.5} pH under clean conditions spanned 2–7, while that under polluted and heavily polluted conditions was mostly concentrated from 3 to 5. Table 1 shows that as the air quality deteriorated, the aerosol component concentration as well as ALWC and H_{air}⁺ all increased in each season. The average PM_{2.5} pH under clean conditions was the highest (Table 1), followed by polluted and heavily polluted conditions in spring, summer, and autumn. In winter, however, the average pH under polluted conditions (4.8 ± 1.0) was the highest.

On clean days, some higher PM_{2.5} pH values (> 6) appeared and were generally accompanied by a higher mass fraction of crustal ions (Mg²⁺ and Ca²⁺). In contrast, lower PM_{2.5} pH (< 3) was often accompanied by a higher mass fraction of SO₄²⁻ and lower mass fraction of crustal ions; such conditions were most obvious in summer (Fig. 4). Under polluted and heavily polluted conditions, the mass fractions of major chemical components were similar, and the difference in PM_{2.5} pH between these two conditions was also small. All of these results indicated that the aerosol

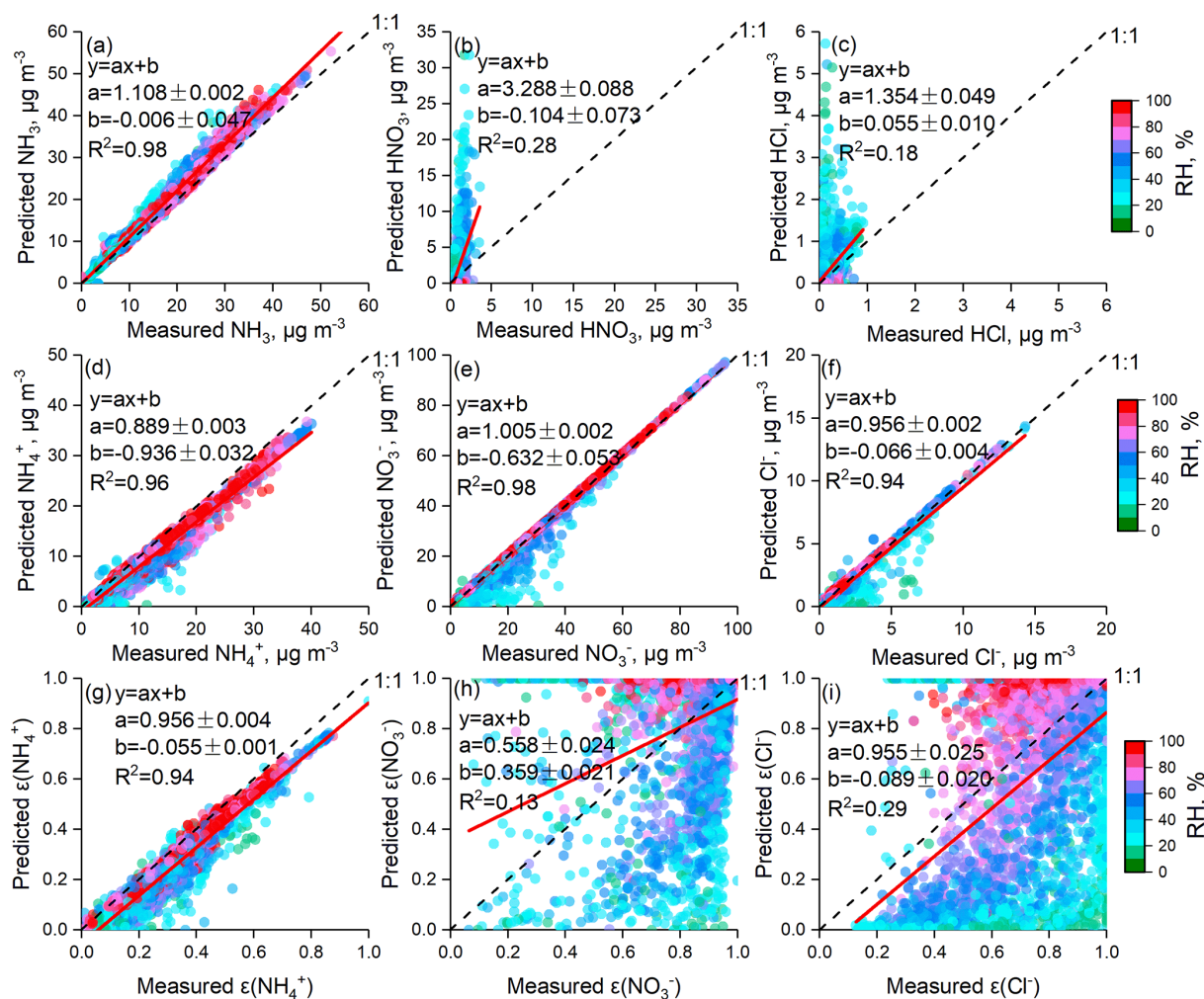


Figure 2. Comparisons of predicted and measured NH_3 , HNO_3 , HCl , NH_4^+ , NO_3^- , Cl^- , $\varepsilon(\text{NH}_4^+)$, $\varepsilon(\text{NO}_3^-)$, and $\varepsilon(\text{Cl}^-)$ colored by RH. In this figure, data from all four seasons were combined; comparisons of individual seasons are shown in Figs. S1–S4 in the Supplement.

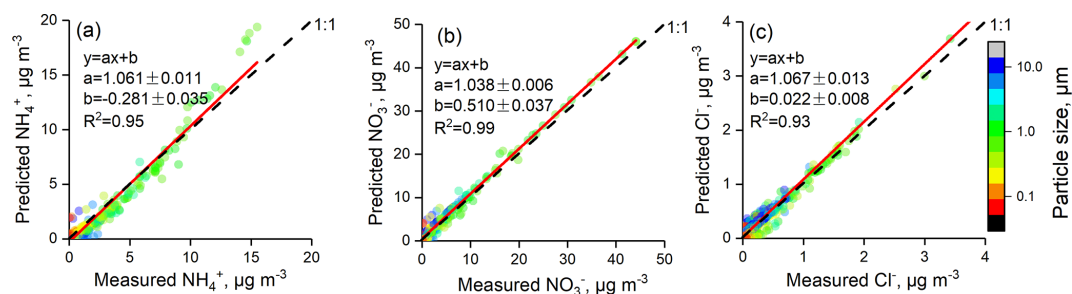


Figure 3. Comparisons of predicted and measured NH_4^+ , NO_3^- , and Cl^- colored by particle size. In this figure, all MOUDI data were combined.

chemical composition should be an essential factor that drives aerosol acidity. The impact of aerosol composition on $\text{PM}_{2.5}$ pH is discussed in Sect. 3.3.

In spring, summer, and autumn, the pH of $\text{PM}_{2.5}$ from the northern direction was generally higher than that from the southwest direction, and the higher pH in summer also oc-

curred with strong southwest winds (wind speed $> 3 \text{ m s}^{-1}$) (Fig. 5). Generally, northern winds occur with cold-front systems, which can sweep away air pollutants but raise dust in which the crustal ion species (Ca^{2+} , Mg^{2+}) are higher. In winter, the $\text{PM}_{2.5}$ pH was distributed relatively evenly in all wind directions, but we surprisingly found that the pH in

Table 1. Average mass concentrations of NO_3^- , SO_4^{2-} , NH_4^+ , and $\text{PM}_{2.5}$, as well as ALWC, H_{air}^+ , and $\text{PM}_{2.5}$ pH, under clean, polluted, and heavily polluted conditions over four seasons.

| Spring | $\text{PM}_{2.5}$ ($\mu\text{g m}^{-3}$) | NO_3^- ($\mu\text{g m}^{-3}$) | SO_4^{2-} ($\mu\text{g m}^{-3}$) | NH_4^+ ($\mu\text{g m}^{-3}$) | ALWC* ($\mu\text{g m}^{-3}$) | $\text{H}_{\text{air}}^+ *$ ($\mu\text{g m}^{-3}$) | pH* |
|------------------|---|---|--|---|-----------------------------------|---|-----------|
| Average | 57 ± 42 | 12.6 ± 14.2 | 8.4 ± 7.7 | 6.7 ± 7.2 | 21 ± 33 | 3.7E-06 ± 1.5E-05 | 4.4 ± 1.2 |
| Clean | 39 ± 19 | 6.6 ± 6.5 | 5.4 ± 3.8 | 3.6 ± 3.2 | 13 ± 23 | 3.2E-06 ± 1.9E-05 | 4.6 ± 1.4 |
| Polluted | 101 ± 21 | 30.7 ± 14.3 | 16.2 ± 6.2 | 15.3 ± 6.0 | 33 ± 36 | 3.1E-06 ± 2.9E-06 | 4.1 ± 0.4 |
| Heavily polluted | 199 ± 62 | 36.4 ± 19.8 | 29.3 ± 14.0 | 23.2 ± 12.3 | 78 ± 60 | 1.6E-05 ± 5.4E-06 | 3.7 ± 0.3 |
| Winter | $\text{PM}_{2.5}$ | NO_3^- | SO_4^{2-} | NH_4^+ | ALWC* | $\text{H}_{\text{air}}^+ *$ | pH* |
| Average | 60 ± 69 | 13.7 ± 21.0 | 7.3 ± 8.7 | 7.3 ± 10.0 | 35 ± 46 | 2.2E-05 ± 2.3E-04 | 4.5 ± 0.7 |
| Clean | 22 ± 20 | 3.6 ± 3.9 | 2.8 ± 1.8 | 2.2 ± 2.0 | 10 ± 16 | 3.2E-07 ± 4.8E-07 | 4.5 ± 0.6 |
| Polluted | 107 ± 21 | 18.9 ± 8.6 | 11.0 ± 5.7 | 11.0 ± 4.7 | 41 ± 45 | 1.9E-05 ± 9.1E-05 | 4.8 ± 1.0 |
| Heavily polluted | 209 ± 39 | 59.7 ± 21.8 | 26.2 ± 6.3 | 29.1 ± 8.7 | 80 ± 52 | 7.0E-05 ± 4.7E-04 | 4.4 ± 0.7 |
| Summer | $\text{PM}_{2.5}$ | NO_3^- | SO_4^{2-} | NH_4^+ | ALWC* | $\text{H}_{\text{air}}^+ *$ | pH* |
| Average | 39 ± 24 | 9.5 ± 9.5 | 8.6 ± 7.5 | 7.2 ± 5.6 | 50 ± 68 | 1.6E-05 ± 1.8E-05 | 3.8 ± 1.2 |
| Clean | 33 ± 18 | 7.3 ± 6.8 | 7.0 ± 6.0 | 5.9 ± 4.0 | 42 ± 61 | 1.4E-05 ± 1.6E-05 | 3.8 ± 1.2 |
| Polluted | 87 ± 13 | 26.5 ± 10.5 | 20.7 ± 7.0 | 17.6 ± 4.8 | 100 ± 88 | 3.1E-05 ± 2.0E-05 | 3.5 ± 0.4 |
| Autumn | $\text{PM}_{2.5}$ | NO_3^- | SO_4^{2-} | NH_4^+ | ALWC* | $\text{H}_{\text{air}}^+ *$ | pH* |
| Average | 59 ± 48 | 18.5 ± 19.5 | 6.5 ± 5.9 | 8.2 ± 8.2 | 109 ± 160 | 8.1E-06 ± 1.1E-05 | 4.3 ± 0.8 |
| Clean | 33 ± 21 | 7.6 ± 7.4 | 4.4 ± 4.1 | 3.8 ± 3.5 | 49 ± 83 | 3.8E-06 ± 6.6E-06 | 4.5 ± 1.0 |
| Polluted | 105 ± 21 | 33.8 ± 11.6 | 14.3 ± 6.3 | 16.0 ± 4.6 | 225 ± 189 | 1.7E-05 ± 1.2E-05 | 4.1 ± 0.3 |
| Heavily polluted | 174 ± 18 | 63.4 ± 15.4 | 25.0 ± 15.9 | 29.0 ± 5.1 | 317 ± 236 | 2.2E-05 ± 1.0E-05 | 4.1 ± 0.2 |

* For data with RH > 30 %.

northerly winds on clean days could be as low as 3–4, which was consistent with the high mass fraction of SO_4^{2-} .

3.2 Diurnal variation in ALWC, H_{air}^+ , and $\text{PM}_{2.5}$ pH

Obvious diurnal variation was observed based on the long-term online dataset, as shown in Fig. 6. To understand the factors that can drive changes in $\text{PM}_{2.5}$ pH, the diurnal variations in NO_3^- , SO_4^{2-} , ALWC, and H_{air}^+ were investigated and are exhibited in Fig. 6. Generally, ALWC was higher during nighttime than daytime and reached a peak near 04:00–06:00 (local time). After sunrise, the increasing temperature resulted in a rapid drop in RH, leading to a clear loss of particle water, and ALWC reached the lowest level in the afternoon. H_{air}^+ was highest in the afternoon, followed by nighttime, and H_{air}^+ was relatively low in the morning. The low ALWC and high H_{air}^+ values in the afternoon resulted in the minimum $\text{PM}_{2.5}$ pH. The average nighttime pH was 0.3–0.4 units higher than that during daytime. From the above discussion, we found that both H_{air}^+ and ALWC had significant diurnal variations, which means that in addition to chemical composition, the $\text{PM}_{2.5}$ pH diurnal variation was also affected by meteorological conditions. This trend is slightly different from in the United States: Guo et al. (2015) found that the ALWC diurnal variation was significant and the diurnal

pattern in pH was mainly driven by the dilution of aerosol water.

The correlation between NO_3^- concentration and $\text{PM}_{2.5}$ pH was weakly positive at low ALWC, and $\text{PM}_{2.5}$ pH was almost independent of the NO_3^- mass concentration at higher ALWC values (Fig. S6). In contrast, at a low ALWC level, increasing SO_4^{2-} decreased the pH; at a high ALWC level, a negative correlation still existed between SO_4^{2-} mass concentration and $\text{PM}_{2.5}$ pH. SO_4^{2-} had a greater effect than NO_3^- on $\text{PM}_{2.5}$ pH.

3.3 Factors affecting $\text{PM}_{2.5}$ pH

In this work, the effects of SO_4^{2-} , TNO_3 , TNH_3 , Ca^{2+} , RH, and T on $\text{PM}_{2.5}$ pH were determined through a four-season sensitivity analysis. The common important driving factors affecting $\text{PM}_{2.5}$ pH variations in all four seasons were SO_4^{2-} , TNH_3 , and T (Table 2), while the unique influencing factors were Ca^{2+} in spring and RH in summer. For ALWC, the most important factor was RH, followed by SO_4^{2-} or NO_3^- . Figures 7 and S7–S14 show how these factors affect the $\text{PM}_{2.5}$ pH, ALWC, and H_{air}^+ over all four seasons.

H_2SO_4 can be completely dissolved in ALWC and in the form of sulfate. As shown in Table 3, HNO_3 also had a high conversion rate to nitrate when RH > 30 %. Under ammonia-rich conditions (defined and explained in Fig. S15), sulfate

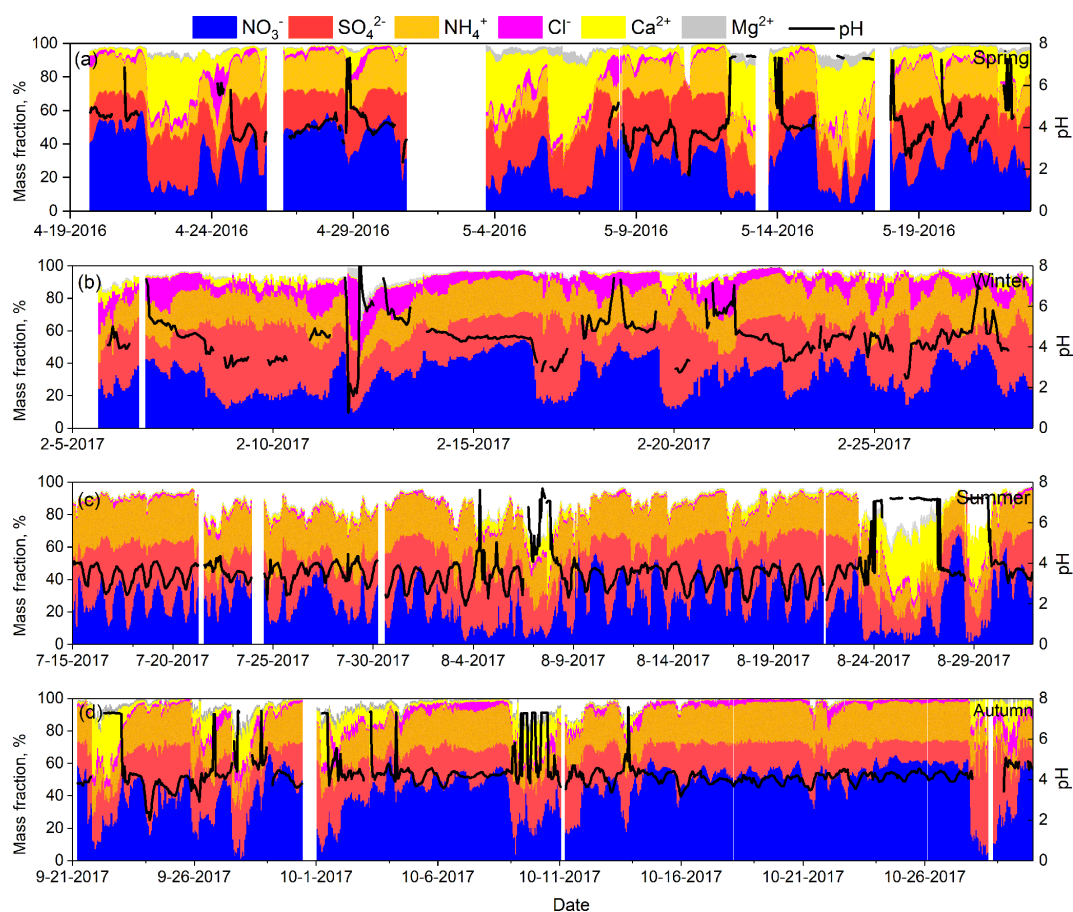


Figure 4. Time series of mass fractions of NO_3^- , SO_4^{2-} , NH_4^+ , Cl^- , Mg^{2+} , and Ca^{2+} with respect to the total ion content, as well as $\text{PM}_{2.5}$ pH in all four seasons ($\text{PM}_{2.5}$ pH values at $\text{RH} \leq 30\%$ were excluded).

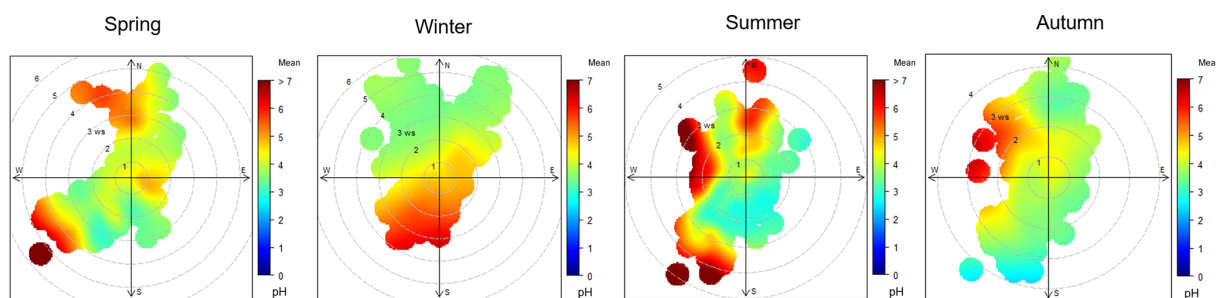


Figure 5. Wind-dependence map of $\text{PM}_{2.5}$ pH over four seasons. In each picture, the shaded contour indicates the mean value of $\text{PM}_{2.5}$ pH for varying wind speeds (radial direction) and wind directions (transverse direction) (data at $\text{RH} \leq 30\%$ were excluded).

and nitrate mostly exist in the aerosol phase with ammonium. The thermodynamic equilibrium between NH_4^+ and NH_3 makes aerosol acidic (Weber et al., 2016). In the sensitivity tests, we found that elevated SO_4^{2-} was crucial in the increase in H_{air}^+ (Table S2, Figs. S7, S9, S12) and ALWC (Table S2, Figs. S8, S10, S13), and had a key role in aerosol acidity (Figs. 7, S11, S14). However, only the $\text{PM}_{2.5}$ pH in winter and autumn decreased significantly with elevated TNO_3 (Figs. 7, S14). In spring and summer, $\text{PM}_{2.5}$ pH changed lit-

tle with elevated TNO_3 . When the TNO_3 concentration was low, $\text{PM}_{2.5}$ pH even increased with elevated TNO_3 (Figs. 7, S11). The effect of TNO_3 on H_{air}^+ and ALWC is similar to that of SO_4^{2-} ; that is, the elevated TNO_3 will also result in the increase in H_{air}^+ and ALWC. The difference is that SO_4^{2-} can lead to a much higher concentration of H_{air}^+ than TNO_3 due to its low volatility (Figs. S7, S9, S12). Thus, the sensitivity of $\text{PM}_{2.5}$ pH to TNO_3 is less than that to SO_4^{2-} . Moreover,

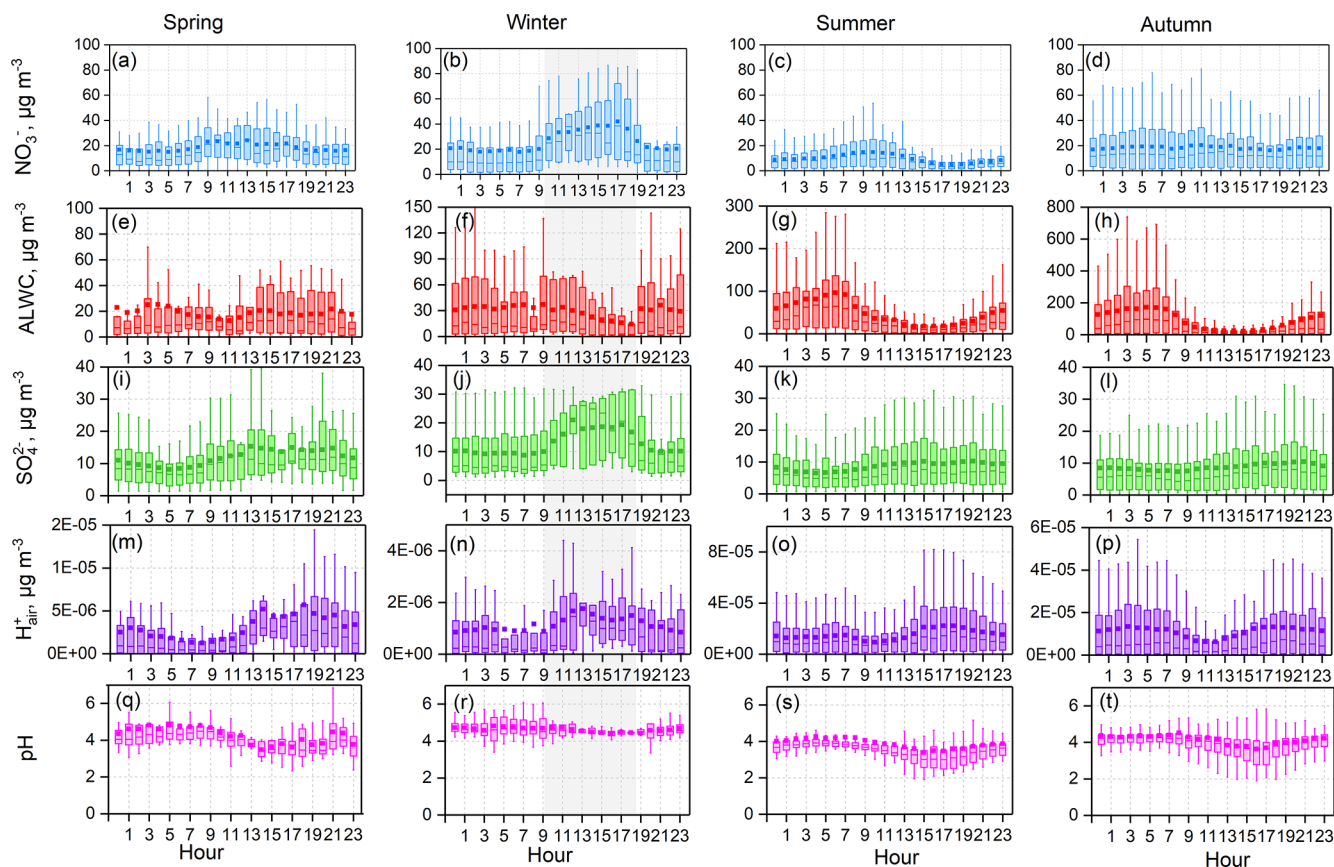


Figure 6. Diurnal patterns of mass concentrations of NO_3^- and SO_4^{2-} in $\text{PM}_{2.5}$, predicted aerosol liquid water content (ALWC), H_{air}^+ , and $\text{PM}_{2.5}$ pH over four seasons. Mean and median values are shown, together with 25 % and 75 % quantiles. Data at $\text{RH} \leq 30\%$ were excluded, and the shaded area represents the time period when most RH values were lower than 30 %.

Table 2. Sensitivity of $\text{PM}_{2.5}$ pH to SO_4^{2-} , TNH_3 , TNO_3 , Ca^{2+} , RH, and T . A larger magnitude of the relative standard deviation (RSD) represents a larger impact derived from variations in variables.

| Impact factor | SO_4^{2-} | TNO_3 | TNH_3 | Ca^{2+} | RH | T |
|---------------|--------------------|----------------|----------------|------------------|-------|-------|
| Spring RSD | 12.4 % | 5.2 % | 3.9 % | 7.5 % | 1.3 % | 7.0 % |
| Winter RSD | 28.1 % | 8.4 % | 27.0 % | 1.0 % | 4.1 % | 6.7 % |
| Summer RSD | 7.9 % | 3.6 % | 8.1 % | 1.9 % | 8.6 % | 5.8 % |
| Autumn RSD | 6.0 % | 3.3 % | 16.1 % | 0.8 % | 2.4 % | 7.5 % |

in spring and summer, more excessive NH_3 could continuously react with the increasing TNO_3 (Table S1), leading to the minimal changes in $\text{PM}_{2.5}$ pH with elevated TNO_3 . Differently, TNH_3 mass concentration was lower in winter and TNO_3 was higher in autumn (Table S1), which made TNH_3 not excessive enough and resulted in the decreased $\text{PM}_{2.5}$ pH with elevated TNO_3 .

In the process of increasing NH_3 concentration in the ammonia–nitric acid–sulfuric acid–water system, NH_3 first reacts with sulfuric acid and consumes a large amount of H^+ , and then reacts with HNO_3 to produce ammonium nitrate (Seinfeld and Pandis, 2016). After most nitric acid is

converted to ammonium nitrate, it is difficult to dissolve more ammonia into aerosol droplets. The sensitivity tests described this mechanism well. Changes in TNH_3 in the lower concentration range had a significant impact on H_{air}^+ and $\text{PM}_{2.5}$ pH, and variations in TNH_3 at higher concentrations could only generate limited pH changes (Figs. 7, S11, S14). The nonlinear relationship between $\text{PM}_{2.5}$ pH and TNH_3 indicates that although NH_3 in the NCP was abundant, the $\text{PM}_{2.5}$ pH was far from neutral.

In this work, $\text{PM}_{2.5}$ pH was lowest in summer but highest in winter, which was consistent with the SO_4^{2-} mass fraction with respect to the total ion content. The SO_4^{2-} mass frac-

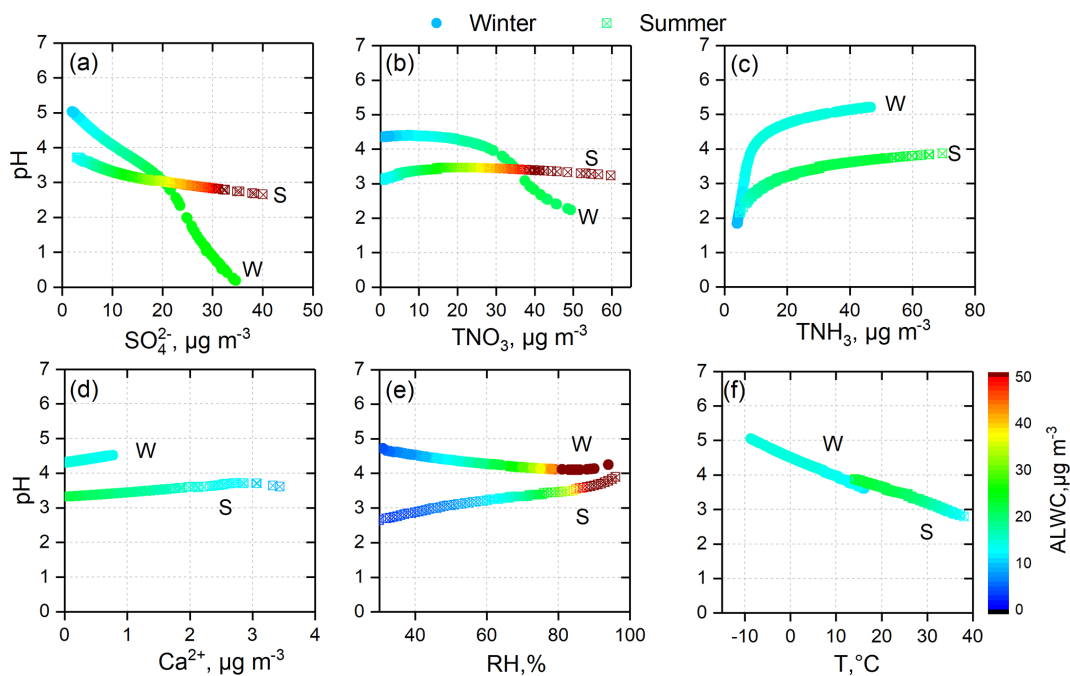


Figure 7. Sensitivity tests of $\text{PM}_{2.5}$ pH to SO_4^{2-} , TNO_3 , TNH_3 , Ca^{2+} , and meteorological parameters (RH and T) in summer (S) and winter (W).

tion was highest in summer among the four seasons, with a value of $32.4\% \pm 11.1\%$, but lowest in winter, with a value of $20.9\% \pm 4.4\%$. In recent years, the SO_4^{2-} mass fraction in $\text{PM}_{2.5}$ in Beijing has decreased significantly due to the strict emission control measures for SO_2 ; in most cases, NO_3^- dominates the inorganic ions (Zhao et al., 2013, 2017; Huang et al., 2017; Ma et al., 2017), which could reduce aerosol acidity. A study in the Pearl River Delta of China showed that the in situ acidity of $\text{PM}_{2.5}$ significantly decreased from 2007 to 2012; the variation in acidity was mainly caused by the decrease in sulfate (Fu et al., 2015). The excessive NH_3 in the atmosphere and the high NO_3^- mass fraction in $\text{PM}_{2.5}$ is the reason why the aerosol acidity in China is lower than that in Europe and the United States (Guo et al., 2017).

Ca^{2+} is an important crustal ion; in the output of ISORROPIA II, Ca exists mainly as CaSO_4 (slightly soluble). Elevated Ca^{2+} concentrations can increase $\text{PM}_{2.5}$ pH by decreasing H_{air}^+ and ALWC (Figs. 7 and S7–S14). As discussed in Sect. 3.1, on clean days, $\text{PM}_{2.5}$ pH reached 6–7 when the mass fraction of Ca^{2+} was high; hence, the role of crustal ions in $\text{PM}_{2.5}$ pH cannot be ignored in areas or seasons (such as spring) in which mineral dust is an important particle source. Due to the strict control measures for road dust, construction sites, and other bare ground, the crustal ions in $\text{PM}_{2.5}$ decreased significantly in the NCP, especially on polluted days.

In addition to the particle chemical composition, meteorological conditions also have important impacts on aerosol acidity. RH had different impacts on $\text{PM}_{2.5}$ pH in different

seasons (Figs. 7, S11, S14). In winter, elevated RH could reduce $\text{PM}_{2.5}$ pH. However, an opposite tendency was observed in summer. In spring and autumn, RH had little impact on $\text{PM}_{2.5}$ pH. Elevated RH can enhance water uptake and promote gas-to-particle conversion, resulting in increased H_{air}^+ and ALWC synchronously for all four seasons. Therefore, the effect of RH on $\text{PM}_{2.5}$ pH depends on the differences in the degree of RH's effect on H_{air}^+ and ALWC. Temperature can alter the $\text{PM}_{2.5}$ pH by affecting gas–particle partitioning. At higher ambient temperatures, $\varepsilon(\text{NH}_4^+)$, $\varepsilon(\text{NO}_3^-)$, and $\varepsilon(\text{Cl}^-)$ all showed a decreased tendency (Figs. 8, S16). The volatilization of ammonium nitrate and ammonium chloride can result in a net increase in particle H^+ and lower pH (Guo et al., 2018). Moreover, a higher ambient temperature tends to lower ALWC, which can further decrease $\text{PM}_{2.5}$ pH.

3.4 Size-resolved aerosol pH

Inorganic ions in particles present clear size distributions, and the size-resolved chemical composition can change at different pollution levels (Zhao et al., 2017; Ding et al., 2017, 2018), which may result in variations in aerosol pH. Thus, we further investigated the size-resolved aerosol pH at different pollution levels. According to the average $\text{PM}_{2.5}$ concentration during each sampling period, all the samples were also classified into three groups (clean, polluted, and heavily polluted) according to the rules described in Sect. 3.1. A severe haze episode occurred during the autumn sampling period; hence, there were more heavily polluted samples in autumn than in other seasons. Figure 9 shows the average size distri-

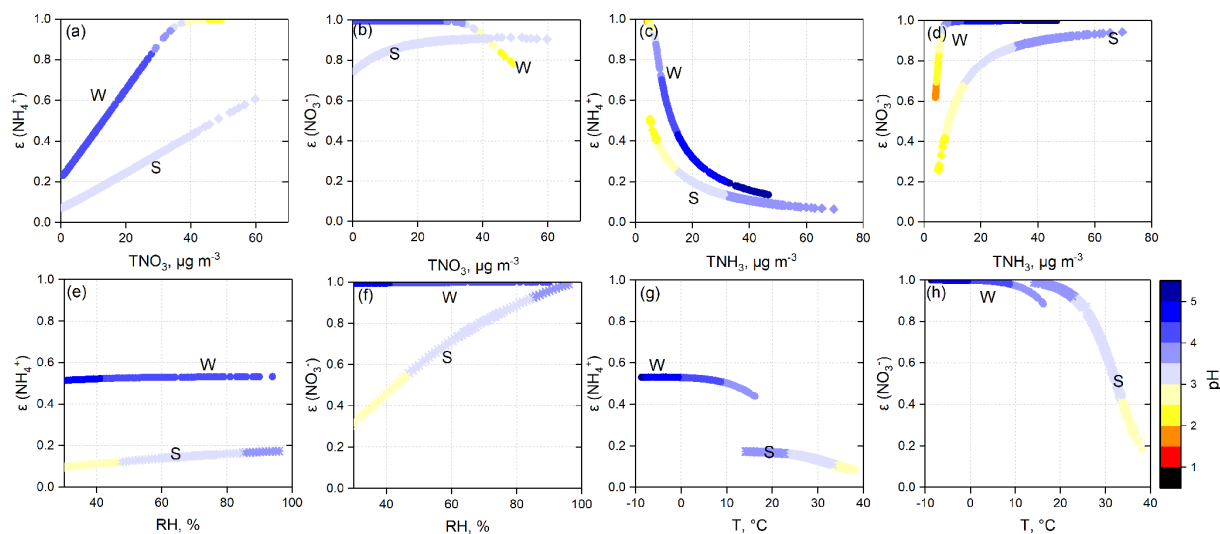


Figure 8. Sensitivity tests of $\epsilon(\text{NH}_4^+)$ and $\epsilon(\text{NO}_3^-)$ to TNO_3 , TNH_3 , RH , and T colored by $\text{PM}_{2.5}$ pH in summer (S) and winter (W).

butions of PM components and pH under clean, polluted, and heavily polluted conditions in summer, autumn, and winter. NO_3^- , SO_4^{2-} , NH_4^+ , Cl^- , K^+ , organic carbon (OC), and elemental carbon (EC) were mainly concentrated in the size range of 0.32–3.1 μm , while Mg^{2+} and Ca^{2+} were predominantly distributed in the coarse mode ($> 3.1 \mu\text{m}$). During haze episodes, the sulfate and nitrate in the fine mode increased significantly. However, the increases in Mg^{2+} and Ca^{2+} in the coarse mode were not as substantial as the increases in NO_3^- , SO_4^{2-} , and NH_4^+ , and the low wind speed made it difficult to raise dust during heavily polluted periods. More detailed information about the size distributions for all analyzed species during the three seasons is given in Zhao et al. (2017) and Su et al. (2018).

The aerosol pH in both the fine mode and coarse mode was lowest in summer among the three seasons, followed by autumn and winter. The seasonal variation in aerosol pH derived from MOUDI data was consistent with that derived from the real-time $\text{PM}_{2.5}$ dataset. In summer, the predominance of sulfate in the fine mode and high ambient temperature resulted in a low pH, ranging from 3.2 to 3.9. The fine-mode aerosol pH in autumn and winter was in the range of 3.9–5.2 and 4.7–5.7, respectively. The fine-mode aerosol pH was overall comparable to the $\text{PM}_{2.5}$ pH. Moreover, in the fine mode, the difference in aerosol pH among size bins was not significant because the aerosol is in thermodynamic equilibrium with the gas phase (Fang et al., 2017). Additionally, the size distributions of aerosol pH in the daytime and nighttime were explored and are illustrated in Fig. S17. In summer and autumn, the pH in the daytime was lower than that in the nighttime, while in winter, the pH was higher in the daytime. During the winter sampling periods, SO_4^{2-} mass fraction was obviously higher in the nighttime and led to abundant H_{air}^+ .

The abundance of Ca^{2+} in the coarse mode led to a predicted aerosol pH approximately at or higher than 7 in autumn and winter. Even if the coarse-mode Ca^{2+} mass concentration in the summer was low, the coarse-mode aerosol pH was still more than 1 unit higher than the fine-mode aerosol pH. The difference in aerosol pH (with and without Ca^{2+}) increased with increasing particle size above 1 μm (Fig. S18). Moreover, the coarse-mode aerosols during severely hazy days shifted from neutral to weakly acidic, especially in autumn and winter. As shown in Fig. 9, the pH in stage 3 (3.1–6.2 μm) declined from 7.4 (clean) to 5.0 (heavily polluted) in winter. The significant decrease in the mass ratio of Ca^{2+} in the coarse-mode particles on heavily polluted days resulted in the loss of acid-buffering capacity. The different size-resolved aerosol acidity levels may be associated with different generation pathways of secondary aerosols. According to Cheng et al. (2016) and Wang et al. (2016), the aqueous oxidation of SO_2 by NO_2 is key in sulfate formation under high-RH and neutral conditions. However, it is speculated that dissolved metals or HONO may be more important for secondary aerosol formation under acidic conditions.

3.5 Factors affecting gas–particle partitioning

Gas–particle partitioning can be directly affected by the concentration levels of gaseous precursors and meteorological conditions. In this work, sensitivity tests showed that decreasing TNO_3 lowered $\epsilon(\text{NH}_4^+)$ effectively, which helped maintain NH_3 in the gas phase. Elevated TNH_3 can increase $\epsilon(\text{NO}_3^-)$ when TNO_3 is fixed, which means that the elevated TNH_3 altered the gas–particle partitioning and shifted more TNO_3 into the particle phase, leading to an increase in nitrate (Figs. 8 and S16). Controlling the emissions of both NO_x (gaseous precursor of NO_3^-) and NH_3 is an efficient way to reduce NO_3^- . However, the relationship between TNH_3 and

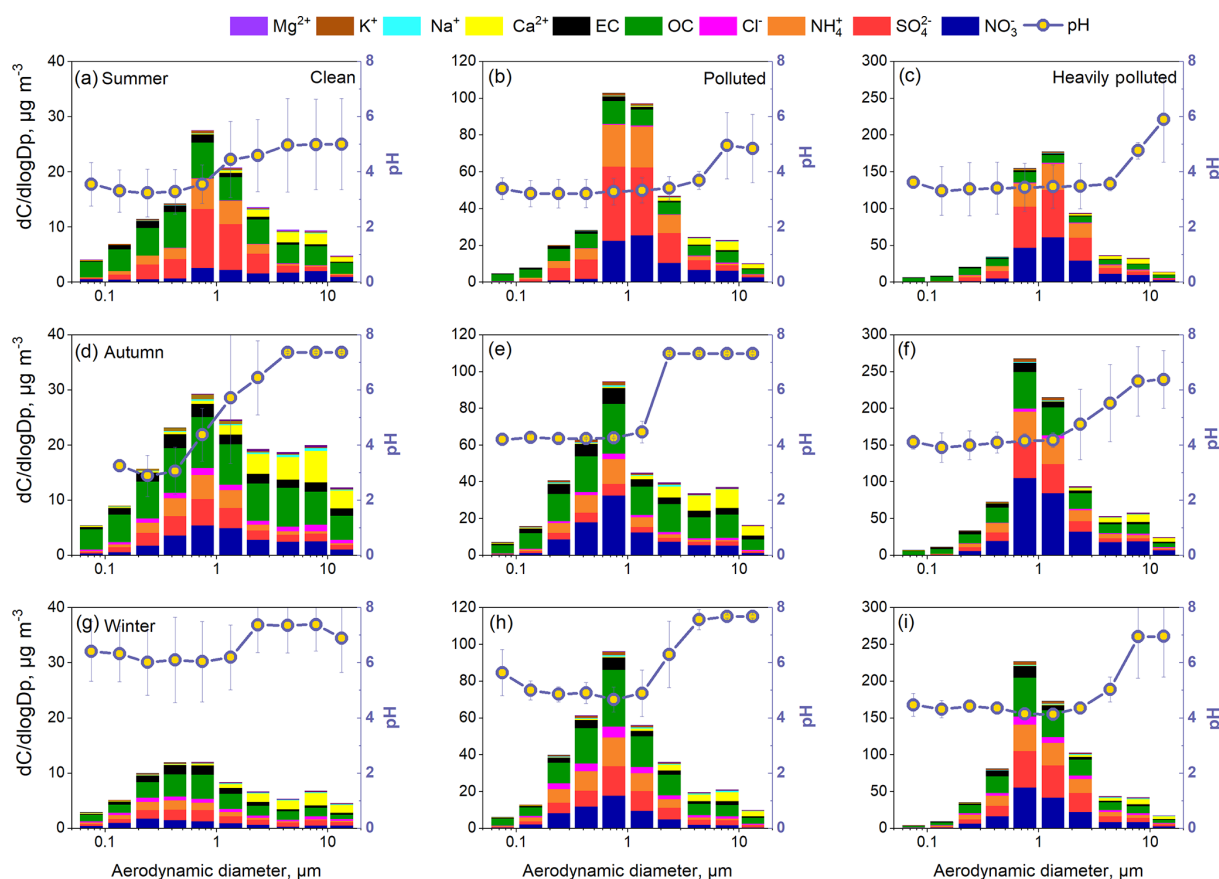


Figure 9. Size distributions of aerosol pH and all analyzed chemical components under clean (a, d, g), polluted (b, e, h), and heavily polluted conditions (c, f, i) in summer, autumn, and winter.

$\varepsilon(\text{NO}_3^-)$ in the sensitivity tests (Figs. 8 and S16) showed that the $\varepsilon(\text{NO}_3^-)$ response to TNH_3 control was highly nonlinear, which means that a decrease in nitrate would happen only when TNH_3 is greatly reduced. The same result was also obtained from a study by Guo et al. (2018). The main sources of NH_3 emission are agricultural fertilization, livestock, and other agricultural activities, which are all associated with people's livelihoods. Therefore, in terms of controlling the generation of nitrate, a reduction in NO_x emissions is more feasible than a reduction in NH_3 emissions.

RH and temperature can also alter gas–particle partitioning. The equilibrium constants for solutions of ammonium nitrate or ammonium chloride are functions of T and RH. The measurement data also showed that lower T and higher RH contribute to the conversion of more TNH_3 , TNO_3 , and TCl into the particle phase (Table 3). When the RH exceeded 60 %, more than 90 % of TNO_3 was in the particle phase for all four seasons. In summer and autumn, more than half of the TNO_3 and TCl was partitioned into the gaseous phase at lower RH conditions (≤ 30 %). In winter, low temperatures favored the existence of NO_3^- and Cl^- in the aerosol phase, and $\varepsilon(\text{NO}_3^-)$ and $\varepsilon(\text{Cl}^-)$ were higher than 75 %, even at low RH. $\varepsilon(\text{NH}_4^+)$ was lower than $\varepsilon(\text{NO}_3^-)$ and $\varepsilon(\text{Cl}^-)$. In

spring, summer, and autumn, the average $\varepsilon(\text{NH}_4^+)$ was still lower than 0.3 even when the RH was >60 %; this trend was associated with excess NH_3 in the NCP. Higher RH and lower temperature are typical meteorological characteristics of haze events in the NCP (Fig. 1), which are favorable conditions for the formation of secondary particles.

4 Summary and conclusions

Long-term high-temporal-resolution $\text{PM}_{2.5}$ pH and size-resolved aerosol pH in Beijing were calculated with ISOR-ROPIA II. In 2016–2017 in Beijing, the mean $\text{PM}_{2.5}$ pH (RH >30 %) over four seasons was 4.5 ± 0.7 (winter) $> 4.4 \pm 1.2$ (spring) $> 4.3 \pm 0.8$ (autumn) $> 3.8 \pm 1.2$ (summer), showing moderate acidity. In this work, both H_{air}^+ and ALWC had significant diurnal variations, indicating that aerosol acidity in the NCP was driven by both aerosol composition and meteorological conditions. The average $\text{PM}_{2.5}$ nighttime pH was 0.3–0.4 units higher than that in the daytime. The $\text{PM}_{2.5}$ pH in northerly wind was generally higher than that in wind from the southwest. Size-resolved aerosol pH analysis showed that the coarse-mode aerosol pH was approximately

Table 3. Average measured $\varepsilon(\text{NH}_4^+)$, $\varepsilon(\text{NO}_3^-)$, and $\varepsilon(\text{Cl}^-)$ based on the real-time MARGA dataset and ambient temperature at different ambient RH levels in four seasons.

| | RH | T , °C | $\varepsilon(\text{NH}_4^+)$ | $\varepsilon(\text{NO}_3^-)$ | $\varepsilon(\text{Cl}^-)$ |
|--------|-------------|----------------|------------------------------|------------------------------|----------------------------|
| Spring | $\leq 30\%$ | 24.8 ± 3.7 | 0.17 ± 0.14 | 0.84 ± 0.12 | 0.67 ± 0.24 |
| | 30 %–60 % | 20.6 ± 3.8 | 0.25 ± 0.14 | 0.91 ± 0.06 | 0.82 ± 0.16 |
| | $> 60\%$ | 15.8 ± 2.7 | 0.28 ± 0.12 | 0.96 ± 0.03 | 0.96 ± 0.06 |
| Winter | $\leq 30\%$ | 5.4 ± 5.3 | 0.31 ± 0.13 | 0.78 ± 0.12 | 0.89 ± 0.14 |
| | 30 %–60 % | 1.0 ± 3.6 | 0.50 ± 0.21 | 0.89 ± 0.10 | 0.97 ± 0.03 |
| | $> 60\%$ | -1.9 ± 2.1 | 0.60 ± 0.20 | 0.96 ± 0.03 | 0.99 ± 0.01 |
| Summer | $\leq 30\%$ | 35.6 ± 0.4 | 0.06 ± 0.02 | 0.35 ± 0.20 | 0.39 ± 0.17 |
| | 30 %–60 % | 29.6 ± 4.2 | 0.17 ± 0.11 | 0.65 ± 0.23 | 0.43 ± 0.16 |
| | $> 60\%$ | 25.2 ± 3.8 | 0.26 ± 0.12 | 0.90 ± 0.12 | 0.71 ± 0.15 |
| Autumn | $\leq 30\%$ | 21.7 ± 7.5 | 0.07 ± 0.06 | 0.49 ± 0.25 | 0.45 ± 0.21 |
| | 30 %–60 % | 20.8 ± 6.3 | 0.21 ± 0.14 | 0.82 ± 0.19 | 0.67 ± 0.21 |
| | $> 60\%$ | 14.9 ± 5.7 | 0.30 ± 0.19 | 0.92 ± 0.10 | 0.86 ± 0.13 |

equal to or even higher than 7 in winter and autumn, which was considerably higher than the fine-mode aerosol pH. The presence of Ca^{2+} had a crucial effect on coarse-mode aerosol pH. Under heavily polluted conditions, the mass fractions of Ca^{2+} in coarse particles decreased significantly, resulting in an evident increase in the coarse-mode aerosol acidity. The $\text{PM}_{2.5}$ pH sensitivity tests also showed that when evaluating aerosol acidity, the role of crustal ions cannot be ignored in areas or seasons (such as spring) where mineral dust is an important particle source. In northern China, dust can effectively buffer aerosol acidity.

The sensitivity tests in this work showed that the common important driving factors affecting $\text{PM}_{2.5}$ pH are SO_4^{2-} , TNH_3 , and T , while unique influencing factors were Ca^{2+} in spring and RH in summer. Owing to the significantly rich NH_3 in the atmosphere, the change in $\text{PM}_{2.5}$ pH was not significant with the elevated TNO_3 , especially in spring and summer. Excess NH_3 in the atmosphere and a high NO_3^- mass fraction in $\text{PM}_{2.5}$ is the reason why aerosol acidity in China is lower than that in Europe and the United States. Notably, TNH_3 had a great influence on aerosol acidity at lower concentrations but had a limited influence on $\text{PM}_{2.5}$ pH when present in excess. The nonlinear relationship between $\text{PM}_{2.5}$ pH and TNH_3 indicated that although NH_3 in the NCP was abundant, the $\text{PM}_{2.5}$ pH was still acidic due to the thermodynamic equilibrium between aerosol droplet and precursor gases. Higher ambient temperature could reduce the $\text{PM}_{2.5}$ pH by increasing ammonium evaporation and decreasing ALWC. RH had different impacts on $\text{PM}_{2.5}$ pH in different seasons, which depends on the differences in the degree of RH's effects on H_{air}^+ and ALWC.

In recent years, nitrates have dominated $\text{PM}_{2.5}$ in the NCP, especially on heavily polluted days. Sensitivity tests showed that decreasing TNO_3 and TNH_3 could lower $\varepsilon(\text{NH}_4^+)$ and $\varepsilon(\text{NO}_3^-)$, helping to reduce nitrate production. However, the

$\varepsilon(\text{NO}_3^-)$ response to TNH_3 control was highly nonlinear. Given that ammonia was excessive in most cases, a decrease in nitrate would occur only if TNH_3 were greatly reduced. Therefore, in terms of controlling the generation of nitrate, a reduction in NO_x emissions is more feasible than a reduction in NH_3 emissions.

Data availability. All data in this work are available by contacting the corresponding author P. S. Zhao (pszhao@ium.cn).

Supplement. The supplement related to this article is available online at: <https://doi.org/10.5194/acp-19-7939-2019-supplement>.

Author contributions. PZ designed and led this study. PZ was responsible for all observations and data collection. JD, PZ, and YZ interpreted the data and discussed the results. JS and XD analyzed the chemical compositions of size-resolved aerosol samples. JD and PZ wrote the paper.

Competing interests. The authors declare that they have no conflict of interest.

Acknowledgements. This work was supported by the National Natural Science Foundation of China (41675131), the Beijing Talents Fund (2014000021223ZK49), and the Beijing Natural Science Foundation (8131003). Special thanks are extended to the Max Planck Institute for Chemistry and Leibniz Institute for Tropospheric Research where Pusheng Zhao visited as a guest scientist in 2018.

Financial support. This research has been supported by the National Natural Science Foundation of China (grant no. 41675131), the Beijing Talents Fund (grant no. 2014000021223ZK49), and the Beijing Natural Science Foundation (grant no. 8131003).

Review statement. This paper was edited by Athanasios Nenes and reviewed by three anonymous referees.

References

- Bian, Y. X., Zhao, C. S., Ma, N., Chen, J., and Xu, W. Y.: A study of aerosol liquid water content based on hygroscopicity measurements at high relative humidity in the North China Plain, *Atmos. Chem. Phys.*, 14, 6417–6426, <https://doi.org/10.5194/acp-14-6417-2014>, 2014.
- Bougiatioti, A., Nikolaou, P., Stavroulas, I., Kouvarakis, G., Weber, R., Nenes, A., Kanakidou, M., and Mihalopoulos, N.: Particle water and pH in the eastern Mediterranean: source variability and implications for nutrient availability, *Atmos. Chem. Phys.*, 16, 4579–4591, <https://doi.org/10.5194/acp-16-4579-2016>, 2016.
- Chen, X., Walker, J. T., and Geron, C.: Chromatography related performance of the Monitor for AeRosols and Gases in ambient air (MARGA): laboratory and field-based evaluation, *Atmos. Meas. Tech.*, 10, 3893–3908, <https://doi.org/10.5194/amt-10-3893-2017>, 2017.
- Cheng, Y. F., Zheng, G. J., Wei C., Mu, Q., Zheng, B., Wang, Z. B., Gao, M., Zhang, Q., He, K. B., Carmichael, G., Pöschl, U., and Su, H.: Reactive nitrogen chemistry in aerosol water as a source of sulfate during haze events in China, *Sci. Adv.*, 2, e1601530, <https://doi.org/10.1126/sciadv.1601530>, 2016.
- Clegg, S. L., Brimblecombe, P., and Wexler, A. S.: A thermodynamic model of the system H^+ , NH_4^+ , SO_4^{2-} , NO_3^- , H_2O at tropospheric temperatures, *J. Phys. Chem.*, 102, 2137–2154, <https://doi.org/10.1021/jp973042r>, 1998.
- Craig, R. L., Peterson, P. K., Nandy, L., Lei, Z., Hossain, M. A., Camarena, S., Dodson, R. A., Cook, R. D., Dutcher, C. S., and Ault, A. P.: Direct determination of aerosol pH: size-Resolved measurements of submicrometer and supermicrometer aqueous particles, *Anal. Chem.*, 90, 11232–11239, <https://doi.org/10.1021/acs.analchem.8b00586>, 2018.
- Ding, J., Zhang, Y. F., Han, S. Q., Xiao, Z. M., Wang, J., and Feng, Y. C.: Chemical, optical and radiative characteristics of aerosols during haze episodes of winter in the North China Plain, *Atmos. Environ.*, 181, 164–176, <https://doi.org/10.1016/j.atmosenv.2018.03.006>, 2018.
- Ding, X. X., Kong, L. D., Du, C. T., Zhanzakova, A., Fu, H. B., Tang, X. F., Wang, L., Yang, X., Chen, J. M., and Cheng, T. T.: Characteristics of size-resolved atmospheric inorganic and carbonaceous aerosols in urban Shanghai, *Atmos. Environ.*, 167, 625–641, <https://doi.org/10.1016/j.atmosenv.2017.08.043>, 2017.
- Eddingsaas, N. C., VanderVelde, D. G., and Wennberg, P. O.: Kinetics and products of the acid-catalyzed ring-opening of atmospherically relevant butyl epoxy alcohols, *J. Phys. Chem. A*, 114, 8106–8113, <https://doi.org/10.1021/Jp103907c>, 2010.
- Engelhart, G. J., Hildebrandt, L., Kostenidou, E., Mihalopoulos, N., Donahue, N. M., and Pandis, S. N.: Water content of aged aerosol, *Atmos. Chem. Phys.*, 11, 911–920, <https://doi.org/10.5194/acp-11-911-2011>, 2011.
- Fang, T., Guo, H. Y., Zeng, L. H., Verma, V., Nenes, A., and Weber, R. J.: Highly acidic ambient particles, soluble metals, and oxidative potential: A link between sulfate and aerosol toxicity, *Environ. Sci. Technol.*, 51, 2611–2620, <https://doi.org/10.1021/acs.est.6b06151>, 2017.
- Fountoukis, C. and Nenes, A.: ISORROPIA II: a computationally efficient thermodynamic equilibrium model for K^+ - Ca^{2+} - Mg^{2+} - NH_4^+ - Na^+ - SO_4^{2-} - NO_3^- - Cl^- - H_2O aerosols, *Atmos. Chem. Phys.*, 7, 4639–4659, <https://doi.org/10.5194/acp-7-4639-2007>, 2007.
- Fountoukis, C., Nenes, A., Sullivan, A., Weber, R., Van Reken, T., Fischer, M., Matias, E., Moya, M., Farmer, D., and Cohen, R. C.: Thermodynamic characterization of Mexico City aerosol during MILAGRO 2006, *Atmos. Chem. Phys.*, 9, 2141–2156, <https://doi.org/10.5194/acp-9-2141-2009>, 2009.
- Fu, X., Guo, H., Wang, X., Ding, X., He, Q., Liu, T., and Zhang, Z.: $\text{PM}_{2.5}$ acidity at a background site in the Pearl River Delta region in fall-winter of 2007–2012, *J. Hazard. Mater.*, 286, 484–492, <https://doi.org/10.1016/j.jhazmat.2015.01.022>, 2015.
- Gao, J. J., Wang, K., Wang, Y., Liu, S. H., Zhu, C. Y., Hao, J. M., Liu, H. J., Hua, S. B., and Tian, H. Z.: Temporal-spatial characteristics and source apportionment of $\text{PM}_{2.5}$ as well as its associated chemical species in the Beijing-Tianjin-Hebei region of China, *Environ. Pollut.*, 233, 714–724, <https://doi.org/10.1016/j.atmosenv.2015.02.022>, 2018.
- Galon-Negru, A. G., Olariu, R. I., and Arsene, C.: Chemical characteristics of size-resolved atmospheric aerosols in Iasi, north-eastern Romania: nitrogen-containing inorganic compounds control aerosol chemistry in the area, *Atmos. Chem. Phys.*, 18, 5879–5904, <https://doi.org/10.5194/acp-18-5879-2018>, 2018.
- Guo, H., Xu, L., Bougiatioti, A., Cerully, K. M., Capps, S. L., Hite Jr., J. R., Carlton, A. G., Lee, S.-H., Bergin, M. H., Ng, N. L., Nenes, A., and Weber, R. J.: Fine-particle water and pH in the southeastern United States, *Atmos. Chem. Phys.*, 15, 5211–5228, <https://doi.org/10.5194/acp-15-5211-2015>, 2015.
- Guo, H. Y., Sullivan, A. P., Campuzano-Jost, P., Schroder, J. C., Lopez-Hilfiker, F. D., Dibb, J. E., Jimenez, J. L., Thornton, J. A., Brown, S. S., Nenes, A., and Weber, R. J.: Fine particle pH and the partitioning of nitric acid during winter in the northeastern United States, *J. Geophys. Res.-Atmos.*, 121, 10355–10376, <https://doi.org/10.1002/2016JD025311>, 2016.
- Guo, H. Y., Weber, R. J., and Nenes, A.: High levels of ammonia do not raise fine particle pH sufficiently to yield nitrogen oxide-dominated sulfate production, *Sci. Rep.*, 7, 12109, <https://doi.org/10.1038/s41598-017-11704-0>, 2017.
- Guo, H., Otjes, R., Schlag, P., Kiendler-Scharr, A., Nenes, A., and Weber, R. J.: Effectiveness of ammonia reduction on control of fine particle nitrate, *Atmos. Chem. Phys.*, 18, 12241–12256, <https://doi.org/10.5194/acp-18-12241-2018>, 2018.
- Hennigan, C. J., Izumi, J., Sullivan, A. P., Weber, R. J., and Nenes, A.: A critical evaluation of proxy methods used to estimate the acidity of atmospheric particles, *Atmos. Chem. Phys.*, 15, 2775–2790, <https://doi.org/10.5194/acp-15-2775-2015>, 2015.
- Huang, X., Liu, Z., Liu, J., Hu, B., Wen, T., Tang, G., Zhang, J., Wu, F., Ji, D., Wang, L., and Wang, Y.: Chemical characterization and source identification of $\text{PM}_{2.5}$ at multiple sites in the Beijing–

- Tianjin–Hebei region, China, *Atmos. Chem. Phys.*, 17, 12941–12962, <https://doi.org/10.5194/acp-17-12941-2017>, 2017.
- Liu, M. X., Song, Y., Zhou, T., Xu, Z. Y., Yan, C. Q., Zheng, M., Wu, Z. J., Hu, M., Wu, Y. S., and Zhu, T.: Fine particle pH during severe haze episodes in northern China, *Geophys. Res. Lett.*, 44, 5213–5221, <https://doi.org/10.1002/2017GL073210>, 2017.
- Ma, Q. X., Wu, Y. F., Zhang, D. Z., Wang, X. J., Xia, Y. J., Liu, X. Y., Tian, P., Han, Z. W., Xia, X. G., Wang, Y., and Zhang, R. J.: Roles of regional transport and heterogeneous reactions in the PM_{2.5} increase during winter haze episodes in Beijing, *Sci. Total Environ.*, 599–600, 246–253, <https://doi.org/10.1016/j.scitotenv.2017.04.193>, 2017.
- Meier, J., Wehner, B., Massling, A., Birmili, W., Nowak, A., Gnauk, T., Brüggemann, E., Herrmann, H., Min, H., and Wiedensohler, A.: Hygroscopic growth of urban aerosol particles in Beijing (China) during wintertime: a comparison of three experimental methods, *Atmos. Chem. Phys.*, 9, 6865–6880, <https://doi.org/10.5194/acp-9-6865-2009>, 2009.
- Meskhidze, N., Chameides, W. L., Nenes, A., and Chen, G.: Iron mobilization in mineral dust: Can anthropogenic SO₂ emissions affect ocean productivity?, *Geophys. Res. Lett.*, 30, 2085, <https://doi.org/10.1029/2003gl018035>, 2003.
- Nenes, A., Pandis, S. N., and Pilinis, C.: ISORROPIA: A new thermodynamic equilibrium model for multiphase multi-component inorganic aerosols, *Aquat. Geochem.*, 4, 123–152, <https://doi.org/10.1023/A:1009604003981>, 1998.
- Nowak, J. B., Huey, L. G., Russell, A. G., Tian, D., Neuman, J. A., Orsini, D., Sjostedt, S. J., Sullivan, A. P., Tanner, D. J., Weber, R. J., Nenes, A., Edgerton, E., and Fehsenfeld, F. C.: Analysis of urban gas phase ammonia measurements from the 2002 Atlanta Aerosol Nucleation and Real-Time Characterization Experiment (ANARChE), *J. Geophys. Res.*, 111, D17308, <https://doi.org/10.1029/2006jd007113>, 2006.
- Pan, X. L., Yan, P., Tang, J., Ma, J. Z., Wang, Z. F., Gbaguidi, A., and Sun, Y. L.: Observational study of influence of aerosol hygroscopic growth on scattering coefficient over rural area near Beijing mega-city, *Atmos. Chem. Phys.*, 9, 7519–7530, <https://doi.org/10.5194/acp-9-7519-2009>, 2009.
- Pathak, R. K., Wang, T., Ho, K. F., and Lee, S. C.: Characteristics of summertime PM_{2.5} organic and elemental carbon in four major Chinese cities: Implications of high acidity for water soluble organic carbon (WSOC), *Atmos. Environ.*, 45, 318–325, <https://doi.org/10.1016/j.atmosenv.2010.10.021>, 2011.
- Peng, C. G., Chan, M. N., and Chan, C. K.: The hygroscopic properties of dicarboxylic and multifunctional acids: Measurements and UNIFAC predictions, *Environ. Sci. Technol.*, 35, 4495–4501, <https://doi.org/10.1021/es0107531>, 2001.
- Rengarajan, R., Sudheer, A. K., and Sarin, M. M.: Aerosol acidity and secondary formation during wintertime over urban environment in western India, *Atmos. Environ.*, 45, 1940–1945, 2011.
- Rumsey, I. C., Cowen, K. A., Walker, J. T., Kelly, T. J., Hanft, E. A., Mishoe, K., Rogers, C., Proost, R., Beachley, G. M., Lear, G., Frelink, T., and Otjes, R. P.: An assessment of the performance of the Monitor for AeRosols and GAs in ambient air (MARGA): a semi-continuous method for soluble compounds, *Atmos. Chem. Phys.*, 14, 5639–5658, <https://doi.org/10.5194/acp-14-5639-2014>, 2014.
- Schwertmann, U. and Cornell, R. M.: Iron Oxides In the Laboratory: Preparation and Characterization, WCH Publisher, Weinheim, <https://doi.org/10.1002/9783527613229>, 1991.
- Seinfeld, J. H. and Pandis, S. N.: Atmospheric Chemistry and Physics: From Air Pollution to Climate Change (3rd edition), John Wiley & Sons, Inc., Hoboken, New Jersey, USA, 2016.
- Shaw, M. A. and Rood, M. J.: Measurement of the crystallization humidities of ambient aerosol particles, *Atmos. Environ.*, 24, 1837–1841, 1990.
- Shi, G. L., Xu, J., Peng, X., Xiao, Z. M., Chen, K., Tian, Y. Z., Guan, X. P., Feng, Y. C., Yu, H. F., Nenes, A., and Russell, A. G.: pH of aerosols in a polluted atmosphere: source contributions to highly acidic aerosol, *Environ. Sci. Technol.*, 51, 4289–4296, <https://doi.org/10.1021/acs.est.6b05736>, 2017.
- Shi, X. R., Nenes, A., Xiao, Z. M., Song, S. J., Yu, H. F., Shi, G. L., Zhao, Q. Y., Chen, K., Feng, Y. C., and Russell, A. G.: High-resolution data sets unravel the effects of sources and meteorological conditions on nitrate and its gas-particle partitioning, *Environ. Sci. Technol.*, 53, 3048–3057, <https://doi.org/10.1021/acs.est.8b06524>, 2019.
- Shi, Z., Bonneville, S., Krom, M. D., Carslaw, K. S., Jickells, T. D., Baker, A. R., and Benning, L. G.: Iron dissolution kinetics of mineral dust at low pH during simulated atmospheric processing, *Atmos. Chem. Phys.*, 11, 995–1007, <https://doi.org/10.5194/acp-11-995-2011>, 2011.
- Song, S., Gao, M., Xu, W., Shao, J., Shi, G., Wang, S., Wang, Y., Sun, Y., and McElroy, M. B.: Fine-particle pH for Beijing winter haze as inferred from different thermodynamic equilibrium models, *Atmos. Chem. Phys.*, 18, 7423–7438, <https://doi.org/10.5194/acp-18-7423-2018>, 2018.
- Su, J., Zhao, P. S., and Dong, Q.: Chemical Compositions and Liquid Water Content of Size-Resolved Aerosol in Beijing, *Aerosol Air Qual. Res.*, 18, 680–692, <https://doi.org/10.4209/aaqr.2017.03.0122>, 2018.
- Surratt, J. D., Chan, A. W., Eddingsaas, N. C., Chan, M., Loza, C. L., Kwan, A. J., Hersey, S. P., Flagan, R. C., Wennberg, P. O., and Seinfeld, J. H.: Reactive intermediates revealed in secondary organic aerosol formation from isoprene, *P. Natl. Acad. Sci. USA*, 107, 6640–6645, <https://doi.org/10.1073/pnas.091114107>, 2010.
- Tan, T. Y., Hu, M., Li, M. R., Guo, Q. F., Wu, Y. S., Fang, X., Gu, F. T., Wang, Y., and Wu, Z. J.: New insight into PM_{2.5} pollution patterns in Beijing based on one-year measurement of chemical compositions, *Sci. Total Environ.*, 621, 734–743, <https://doi.org/10.1016/j.scitotenv.2017.11.208>, 2018.
- Tian, S. L., Pan, Y. P., Liu, Z. R., Wen, T. X., and Wang, Y. S.: Size-resolved aerosol chemical analysis of extreme haze pollution events during early 2013 in urban Beijing, China, *J. Hazard. Mater.*, 279, 452–460, <https://doi.org/10.1016/j.jhazmat.2014.07.023>, 2014.
- Wang, G., Zhang, R., Gomez, M. E., Yang, L., Levy Zamora, M., Hu, M., Lin, Y., Peng, J., Guo, S., Meng, J., Li, J., Cheng, C., Hu, T., Ren, Y., Wang, Y., Gao, J., Cao, J., An, Z., Zhou, W., Li, G., Wang, J., Tian, P., Marrero-Ortiz, W., Secrest, J., Du, Z., Zheng, J., Shang, D., Zeng, L., Shao, M., Wang, W., Huang, Y., Wang, Y., Zhu, Y., Li, Y., Hu, J., Pan, B., Cai, L., Cheng, Y., Ji, Y., Zhang, F., Rosenfeld, D., Liss, P. S., Duce, R. A., Kolb, C. E., and Molina, M. J.: Persistent sulfate formation from London Fog

- to Chinese haze, *P. Natl. Acad. Sci. USA*, 113, 13630–13635, <https://doi.org/10.1073/pnas.1616540113>, 2016.
- Wang, X., Jing, B., Tan, F., Ma, J., Zhang, Y., and Ge, M.: Hygroscopic behavior and chemical composition evolution of internally mixed aerosols composed of oxalic acid and ammonium sulfate, *Atmos. Chem. Phys.*, 17, 12797–12812, <https://doi.org/10.5194/acp-17-12797-2017>, 2017.
- Weber, R. J., Guo, H., Russell, A. G., and Nenes, A.: High aerosol acidity despite declining atmospheric sulfate concentrations over the past 15 years, *Nat. Geosci.*, 9, 282–285, <https://doi.org/10.1038/NGEO2665>, 2016.
- Young, A. H., Keene, W. C., Pszenny, A. A. P., Sander, R., Thornton, J. A., Riedel, T. P., and Maben, J. R.: Phase partitioning of soluble trace gases with size-resolved aerosols in near-surface continental air over northern Colorado, USA, during winter, *J. Geophys. Res.-Atmos.*, 118, 9414–9427, <https://doi.org/10.1002/jgrd.50655>, 2013.
- Zhang, H., Cheng, S., Li, J., Yao, S., and Wang, X.: Investigating the aerosol mass and chemical components characteristics and feedback effects on the meteorological factors in the Beijing-Tianjin-Hebei region, China, *Environ. Pollut.*, 244, 495–502, <https://doi.org/10.1016/j.envpol.2018.10.087>, 2019.
- Zhang, Y., Lang, J., Cheng, S., Li, S., Zhou, Y., Chen, D., Zhang, H., and Wang, H.: Chemical composition and sources of PM₁ and PM_{2.5} in Beijing in autumn, *Sci. Total Environ.*, 630, 72–82, <https://doi.org/10.1016/j.scitotenv.2018.02.151>, 2018.
- Zhao, P. S., Dong, F., He, D., Zhao, X. J., Zhang, X. L., Zhang, W. Z., Yao, Q., and Liu, H. Y.: Characteristics of concentrations and chemical compositions for PM_{2.5} in the region of Beijing, Tianjin, and Hebei, China, *Atmos. Chem. Phys.*, 13, 4631–4644, <https://doi.org/10.5194/acp-13-4631-2013>, 2013.
- Zhao, P. S., Chen, Y. N., and Su, J.: Size-resolved carbonaceous components and water-soluble ions measurements of ambient aerosol in Beijing, *J. Environ. Sci.*, 54, 298–313, <https://doi.org/10.1016/j.jes.2016.08.027>, 2017.
- Zou, J. N., Liu, Z. R., Hu, B., Huang, X. J., Wen, T. X., Ji, D. S., Liu, J. Y., Yang, Y., Yao, Q., and Wang, Y. S.: Aerosol chemical compositions in the North China Plain and the impact on the visibility in Beijing and Tianjin, *Atmos. Res.*, 201, 235–246, <https://doi.org/10.1016/j.atmosres.2017.09.014>, 2018.